FULL PAPER

ADVANCED
FUNCTIONAL
MATERIALS

www.afm-journal.d

Check for
updates

Reconfigurable and Latchable Shape-Morphing Dielectric Elastomers Based on Local Stiffness Modulation

*Bekir Aksoy and Herbert Shea**

Programmable soft materials exhibiting dynamically reconfigurable, reversible, fast, and latchable shape transformation are key for applications ranging from wearable tactile actuators to deployable soft robots. Multimorph soft actuator sheets with high load-bearing capacity are reported, capable of bending on multiple axis, made by combining a single dielectric elastomer actuator (DEA) with two layers of shape memory polymers (SMPs) fibers and an array of stretchable heaters. The rigidity of the SMP fibers can be reduced by two orders of magnitude by Joule heating, thus allowing the orientation and location of soft and hard regions to be dynamically defined by addressing the heaters. When the DEA is then actuated, it bends preferentially along the soft axis, enabling the device to morph into multiple distinct configurations. Cooling down the SMPs locks these shape changes into place. A tip deflection angle of over 300° at 5 kV is achieved with a blocking force of over 27 mN. Devices using two antagonistic DEAs are also reported that attain more complex shapes. Multimorphing is demonstrated by gripping objects with different shapes. An analytical model is developed to determine the design parameters that offers the best trade-off between large actuation and high holding forces.

1. Introduction

Shape-programmable matter refers to a class of active materials whose geometry can be controlled by stimuli such as heat,[1] light,[2] and magnetic[3] and electric fields[4] to achieve or augment a broad range of functional mechanisms such as grippers, mobile robots, or drug delivery systems. Unlike their rigid counterparts, programmable soft materials[5] designed for dynamically reconfigurable shape transformations enable seemingly simple structures to perform complex tasks, for example, origami-inspired surface morphing was used for

crawling robots that can fold themselves,[6] tactile displays capable of controlling both the geometry and the mechanical properties allowed more realistic haptic sensations,[7] self-folding mechanism in microscale was utilized for encapsulation and delivery of drugs.[8] A single material system that combines shape reconfigurability, reversibility, speed, and latching would enable complex functional mechanisms, yet has proven very challenging to develop. Such an active material requires spatial stiffness tuning to reconfigure soft actuators for multiple distinct shapes, an integrated addressing system for stiffness or actuation control, suitable active material, and appropriate design method to reach simultaneously large deformation and high load-bearing capacity. We report here a multistable and reconfigurable shape-morphing sheets combining a dielectric elastomer actuator (DEA) with thermoresponsive shape memory polymers (SMPs) activated by an array of stretchable heaters (**Figure 1**). This active sheet addresses the above-mentioned challenges.

Soft stimuli-responsive materials developed for shape programming can be classified into five main groups: ionic electroactive polymers (IEAPs), hydrogels, liquid crystalline elastomers (LCEs), DEAs, and shape memory polymers.[9] IEAPs respond directly to electric fields, with an actuation based on transport of ions within a polymer membrane. They can generate deformations using low driving voltages, leading to research in possible biomedical applications.[10] Due to their low coupling efficiency, their electromechanical performance has been insufficient for practical applications.[9] Hydrogels undergo reversible large volume changes of up to several times of their initial volumes by swelling-shrinking when subjected to a wide range of external stimuli, for example, ion concentration, pH, heat, light, and electric field.[11] Due to their similarities to living organisms (namely wet and soft), they have been of interest for biomimetic structures. However, they can only operate in aqueous environments, require mass transport of the solvent, and have a response time of order several minutes, and thus poorly suited for many robotic applications. LCEs obtain their shape transformation by changing the direction of their molecular order when exposed to different stimuli, often temperature.[12] They can perform in dry and wet environments with reversible large deformations, with directional strains of up to 400%.[13] During the fabrication, their actuation

B. Aksoy, Prof. H. Shea
Soft Transducers Laboratory (LMTS)
Ecole Polytechnique Fédérale de Lausanne (EPFL)
Neuchâtel 2000, Switzerland
E-mail: herbert.shea@epfl.ch

The ORCID identification number(s) for the author(s) of this article can be found under https://doi.org/10.1002/adfm.202001597.
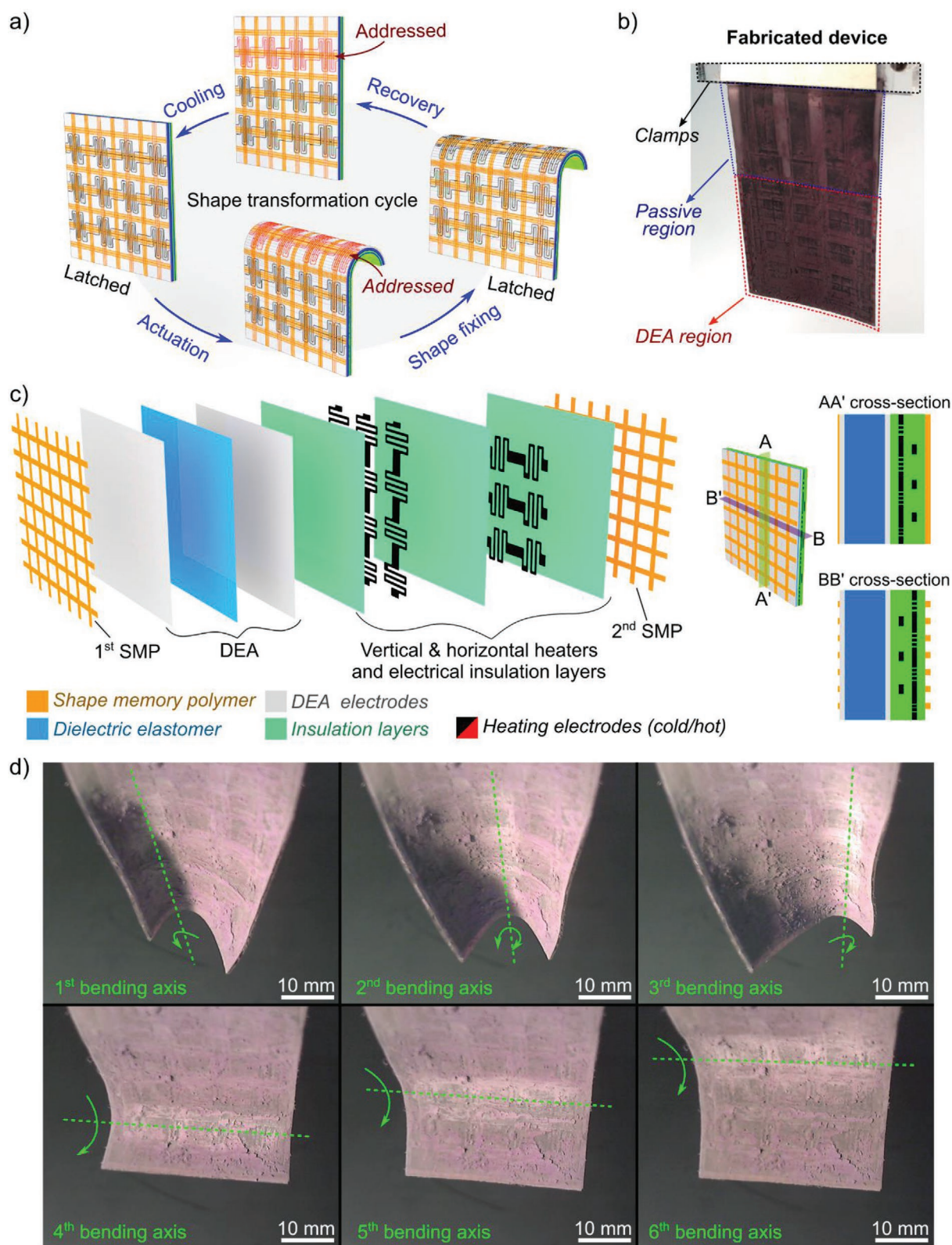
Figure 1. The working mechanism and the layers of the multistable reconfigurable dielectric elastomer sheets. a) The shape transformation cycle showing bending about a Joule-heated soft axis. The hot and cold heaters are colored red and black. b) A photograph of an as-fabricated device showing the active and passive regions. Total thickness is 560 µm. c) The multistable dielectric elastomer sheet consists of a DEA, two sets of vertical and horizontal heaters separated by the insulation layers, and two SMP grids. The schematics on the right show the cross-section view of the dielectric elastomer sheet. d) Photographs of six different latched states.

**ADVANCED
SCIENCE NEWS**
www.advancedsciencenews.com

**ADVANCED
FUNCTIONAL
MATERIALS**
www.afm-journal.de

shape can be programmed by preparing them with local variation in the director orientation.[5c,14] The force generated by LCEs is generally limited by the film thickness; the thicker the film, the higher the force. However, increasing their thicknesses reduces the achievable deformations and increases the fabrication complexity of localizing the alignment of these materials, a requirement to achieve complex deformations. DEAs are electrostatically driven actuators that can generate very large deformations[15] and are to date, the most widely used electroactive polymers.[9] They have been developed for numerous applications such as mobile soft robots capable of working in different environments,[16] tunable optics,[17] pumps,[18] wearable haptics,[19] manipulation of delicate objects,[20] or studying cell mechanics.[21] The electric field needed to actuate DEAs is around 20 V μm^{-1} to 150 V μm^{-1}, which implies a voltage of several kilovolts for typical elastomer membrane thicknesses, though lower operating voltages have been reported.[16d]

These first four categories of stimuli-responsive materials do not inherently exhibit any shape fixation abilities. Mechanically latching them would eliminate the need of applying continuous power to hold a position, enabling more energy efficient soft systems and in most cases longer lifetime. SMPs, on the other hand, can repeatedly hold a temporary deformed shape and then recover their permanent shape upon application of an external stimulus.[22] Thermal programming of SMPs has been the most widely utilized approach in robotics thanks to convenient triggers such as photothermal and Joule heating. The stiffness of thermoresponsive SMPs can be tuned by sweeping the temperature across their glass transition (T_G) region to switch from a soft hot state for easy deformation to a hard cold state (latched state) for high load-bearing.[23] Despite their distinctive function and shape control, most SMPs have one-way shape memory effect, and thus they need to be reprogrammed through external loading for each deformation.

An effective approach to achieve a reversible multistable shapes is to combine shape memory polymers with another stimuli-responsive material, that is, SMP + IEAP[24] or SMP+DEAs.[23a] For this reason, SMPs have previously been combined with soft actuators to create integrated latching mechanisms.[7c,22b,25] However, these systems cannot be reconfigured to achieve multiple distinct configurations. Recently, Ze et al. combined low-coercivity (for heating) and high-remanence (for actuation) magnetic particles with the shape memory polymers to achieve locking and unlocking of multiple deformations.[22c] The magnetization profile of these particles, however, needs to be reprogrammed at high magnetic fields to achieve different configurations under the same external field.[3,22c]

In this work, we introduce multistable and reconfigurable shape-morphing DEA sheets by combining the DEA with heat-activated SMPs and an array of soft stretchable heaters. The SMPs serve as dynamically reconfigurable boundary conditions. The mechanical boundary conditions for DEA fabrication play a defining role the deformation the DEA will generate. They are typically defined during device fabrication. Boundary conditions include, for example, incorporating stiff fibers [20a,26] and bonding the dielectric elastomers to rigid or flexible frames.[27] Another way to change DEA actuation shape is to use a set of electrodes with varying geometries to generate out of plane

motions.[28] Multilayer fabrication of stacked electrodes with different shapes can produce multiple shape morphs according to which set of electrodes the voltage is applied to.[28b] Multisegmented structures can achieve different deformations based on which section is electrostatically addressed.[28a,29]

This work uses stiff fibers to control DEA motion direction, but implement the fibers with stiffness tunable SMPs to morph DEA sheets into multiple distinct configurations. The SMP layer acts as dynamically reconfigurable 2D array of fibers (Figure 1). By locally heating the SMP, we soften only specific fibers (or portions of fibers), thus defining a temporary soft axis about which the bending preferentially occurs when a voltage is applied to the dielectric elastomer sheet. Multiple distinct configurations are obtained by heating different regions and by choosing the sequence of heating and actuation. After the deformation is achieved, the SMPs are cooled down to lock in the deformed shape, enabling zero-power actuated states. Upon cooling, the SMPs become over 200 times stiffer, increasing substantially the load-bearing capacity. Their ability to withstand external loads in the latched states depends on the thickness of the individual SMP layers and the distance between them (i.e., bending moment of inertia). Devices with thicker SMP layers have however less actuation deformation. We developed an analytical model to determine the optimum SMP thicknesses and SMP film positions that offers the best trade-off between large actuation deformation and high holding forces. The model includes up to 11 layers and accurately predicts the behavior of the multistable dielectric elastomer sheet at the actuation, latched, and load-bearing states without using any fitting parameters. The latched zero-power state is >4 times stiffer than the devices at the soft actuated states.

2. Results and Discussion

We report below two examples of complex shape morphing from a thin sheet, first using only one DEA, then using two antagonistic DEAs to generate more complex shapes. We then present and experimentally validate a model for deformation and holding force.

2.1. Shape Morphing and Latching through Localized Stiffness Modulation of Shape Memory Polymers

The multistable shape morphing mechanism is illustrated in Figure 1a. It consists of a DEA (a dielectric membrane and two compliant electrodes), two sets of vertical and horizontal heaters, two SMP grids, and electrical insulation layers. The heaters provide the thermal stimulus needed for the softening and the shape recovery. The orientation of the heaters defines the soft axis of bending, and thus ultimately the possible deformed configurations.

When specific segments of the SMPs are softened by the Joule heating, a temporary soft axis is created, about which the DEA-induced bending occurs when the DEA voltage is applied. To visualize the soft and stiff regions in the device in Figure 1a, the addressed (hot) and the unaddressed (cold) heaters are colored red and black. When the voltage is applied to the DEA electrodes, only the region in the vicinity of the addressed heater

**ADVANCED
SCIENCE NEWS**
www.advancedsciencenews.com

**ADVANCED
FUNCTIONAL
MATERIALS**
www.afm-journal.de

bends. The DEA cannot significantly deform the unheated regions. The SMPs are then allowed to cool, locking the device into a stable deformed configuration (referred as temporary shape). The permanent flat shape can be simply recovered by reheating. This device can be reconfigured for another shape transformation by addressing different heaters. Total thickness of the device is 560 µm; more details are in Section 4.

Figure 1c shows the layers of the structure, with heater configured for six possible shape transformations. With a different patterning of the heaters, we can introduce different regions of deformations within the elastomer sheet for additional morphological transformations. Figure S1, Supporting Information, shows the deformations around two diagonal axes when the diagonally oriented heaters are addressed.

To morph the dielectric elastomer sheet shown in Figure 1b to reach the shapes shown in Figure 1d, we first heated the left vertical segment of the device to 85 °C, followed by applying 6.25 kV across the dielectric membrane to bend this soft segment (a lower voltage could be applied if less bending is desired). Once bent, the applied voltage was maintained at 6.25 kV while the device was allowed to cool for 30 s. This is the shape fixing (or shape programming) step where the device is locked in the actuated state. We turned off the high voltage after the shape fixation, yielding the zero-power actuated position, the first image in Figure 1d. This shape is stable as long as the temperature remains below the T_G of the SMP. The permanent (i.e., initial as fabricated) flat shape was then recovered by heating the device to 85 °C for 30 s. The shape morphing cycle was repeated for the other five segments. Figure 1d shows the deformed images of six latched configurations. The dashed green lines indicate the soft axes created during the actuation. By combining spatial stiffness tuning technique with the shape memory effect in the dielectric elastomer sheets, one can achieve a continuous deformation in various directions without the need of complex joint mechanisms and can hold a given actuated position with zero power.

2.2. Complex Shapes Based on Sequential Deform-and-Hold Operations

We integrate a second DEA in an antagonistic configuration to enable more complex shape transformations, with both positive and negative curvature, using a sequence of deform-and-hold operations of different segments. We report a sheet that can morph, amongst other configurations, into "S" and its mirror "Ƨ" shapes. The operating cycle is schematically demonstrated in **Figure 2**a. First, the right-hand side of the device is deformed with a forward bending and locked in place. Then, the flat left-hand side of the device is bent in the opposite direction of the first bending (backward bending) and subsequently latched. The deformation of the right segment is preserved during the second shape transformation thanks to the cold SMPs in this region. This way, we can decouple the deformations of two neighbor segments and therefore can achieve a deformed S-shape with the left and the right parts having the opposite shapes.

We implemented two DEAs in a dielectric elastomer sheet to adopt an antagonistic behavior. This was achieved by placing two identical DEAs on opposite sides of the stacked layers. The device had two SMP grids, a layer with three vertical heaters, and two antagonistic DEA layers, placed to enable forward and backward bending (Figure 2b).

Figure 2c shows two complex mirror shapes obtained in a single dielectric elastomer sheet. We first softened the left-hand side of the device (≈75 °C) by addressing the left-column heater and applying a voltage of 5.5 kV to the first DEA, which in return only bent the left segment in the backward direction. This deformation was fixed by cooling the SMPs. Subsequently, we simultaneously softened the right segment and electrostatically actuated the second DEA. This generated a forward bending in the right-hand side of the device. Following another shape fixation after the second actuation, we latched the device in an S-shape configuration (see the first image in Figure 2c). The mirror shape of this deformation (Ƨ-shape) was achieved by swapping the synchronization of the DEA actuation and the addressing of the Joule heaters. For this, the actuation of the first DEA is synchronized with the right-column Joule heater, and similarly the second DEA with the left-column heater. As these DEAs have antagonistic behavior, the Maxwell stress generated during the second actuation tries to unfold the deformation of the first segment. However, The SMPs in this region are cold (hence stiff) and they can resist this unfolding force. As depicted from the experimental photographs shown in Figure 2c, the cold SMPs hold the deformed shape under the Maxwell stress.

2.3. Design Principles and Analytical Modeling to Maximize Both Actuation Deformation and Holding Force

The active sheets consist of up to 11 layers of elastomer, compliant electrode, insulation, and SMP. The thickness of each layer and the order of the layers (e.g., SMP at center or at outer layer, one or two SMP layers, heaters inside or outside; see Figure S4, Supporting Information, for three examples of stacks) plays a central role in obtaining both high bending angles and high holding force. Thicker SMP layers enable higher bending stiffness in the cold state, and thus higher load carrying ability. But due to their non-zero stiffness in the hot state, thicker SMP layers reduce the actuation deformation.

We developed an analytical model to quantify the trade-off between large actuation bending and high holding force. The model helps determine the optimum design parameters of the sheets (SMP and DEA film thicknesses and layer order). The model computes bending angle in three different states: 1) the actuation state with the DEA voltage on and the selected heaters on, 2) the latched state where the deformation is held by the cold SMPs (DEA is off), and 3) the load-bearing state where an external force is applied to the latched device, that is, the latched state with a load.

When a voltage is applied across the DEA, it expands laterally, thus applying a bending moment to all layers, hence generating curvature in the sheet. The beam bending was analyzed using Stoney's equations for the mechanical equilibrium.[30] We assumed that the Maxwell stress was uniform and remained constant during the deformation. The strain generated was small enough (<0.10) to use a linear elasticity model. We used
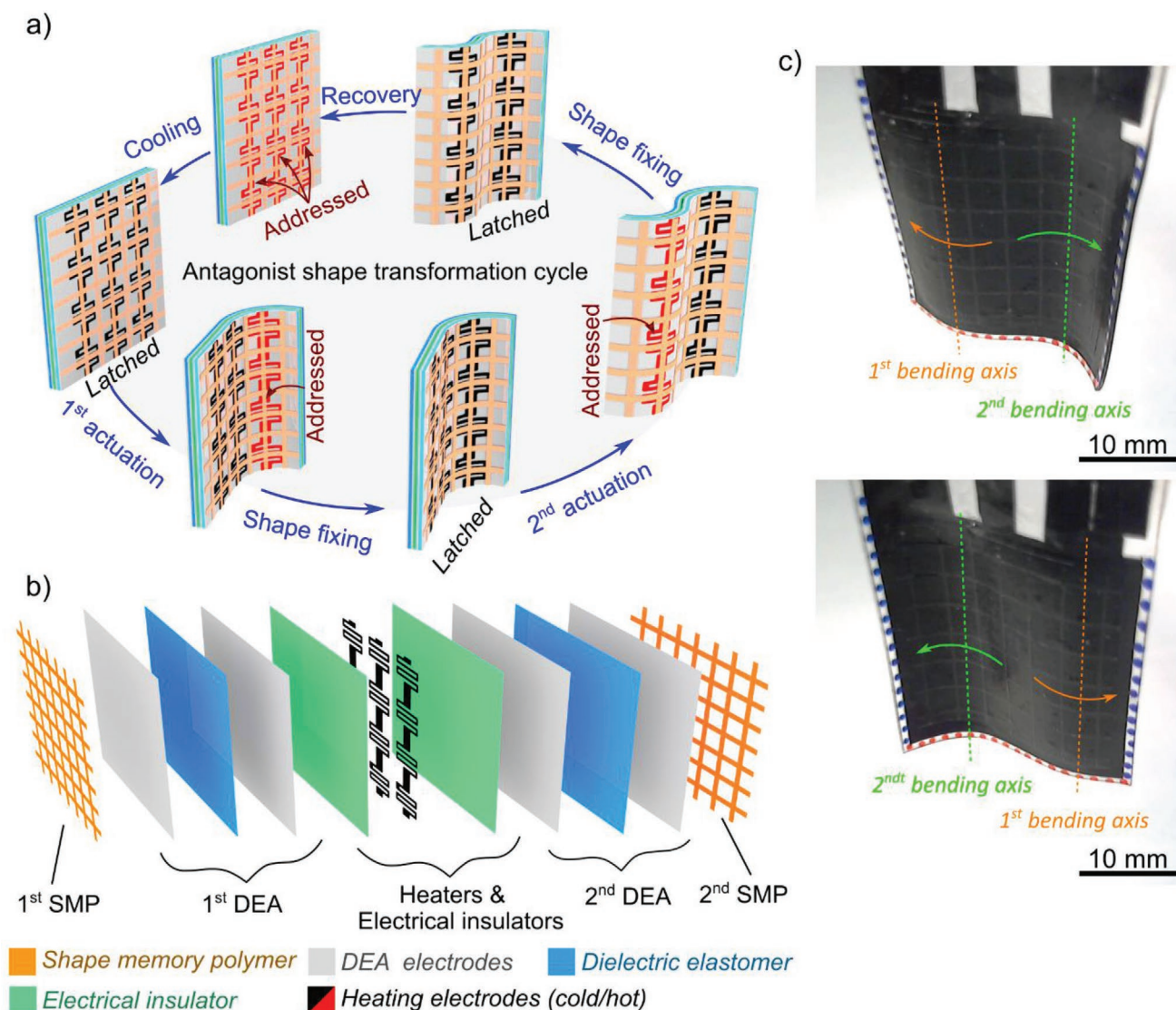
Figure 2. Complex mirror deformations are achievable by synchronizing the electrostatic actuation of the two antagonistic DEAs and the addressing of the Joule heaters. a) The shape transformation cycle showing the sequence of the deform-and-hold operations to achieve S-shape deformation. b) The antagonistic dielectric elastomer sheet consists of two DEAs placed on the opposite sides of a central a set of vertical heaters, and two SMP grids on the outside. It has a thickness of 775 µm. c) Photographs showing the morphing of the flat sheet into two mirror shapes.

the force equilibrium in the tangential direction and moment equilibrium about the z-axis (**Figure 3**a). The elastic force due to the deformation of all layers is equal to the force generated by the voltage applied to the dielectric membrane. Adopting the ideal dielectric elastomer model, we can write the equation of the force equilibrium in the tangential direction as [30,31]
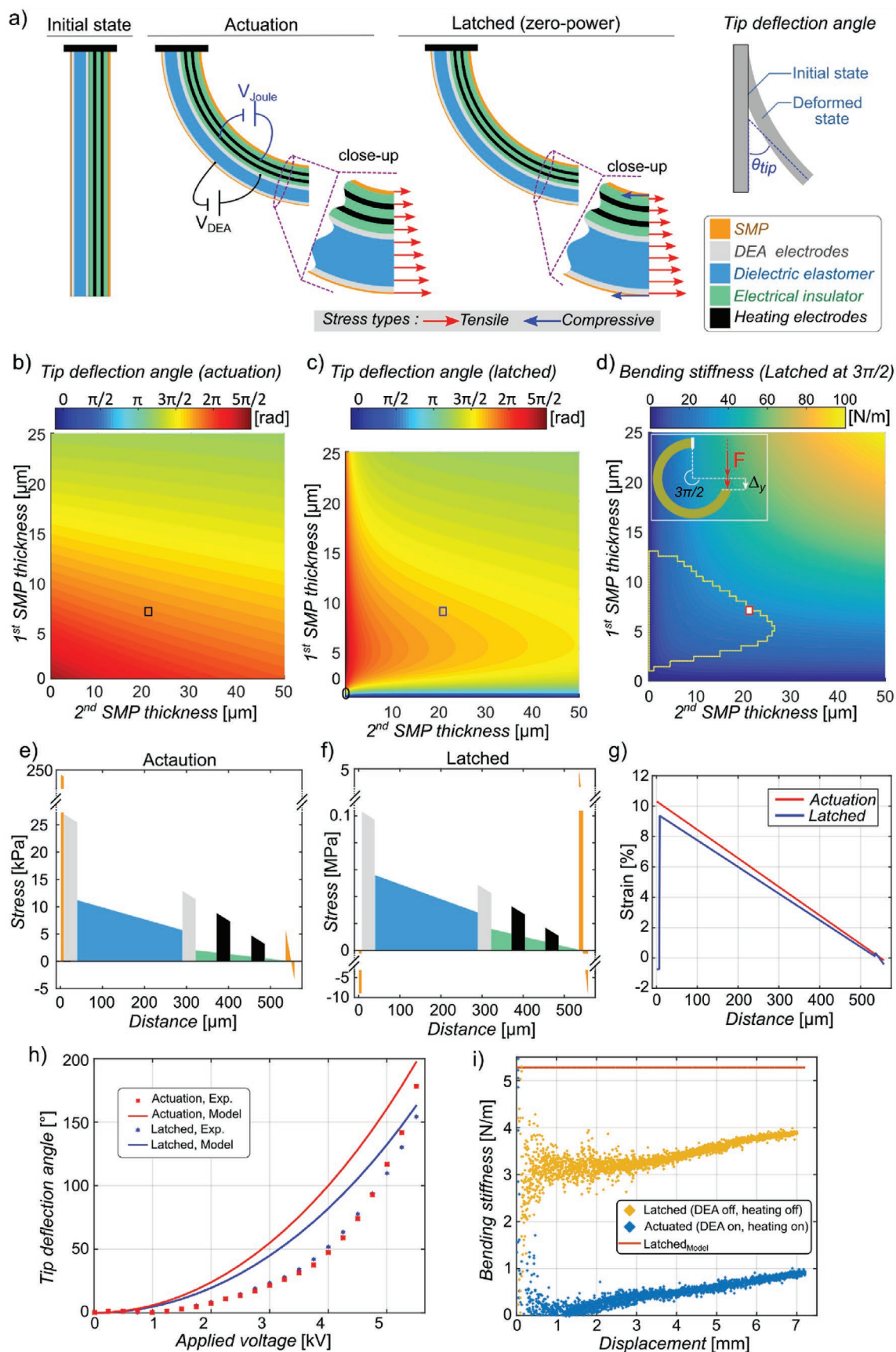
$$\int_{A_{all}} \left(-Y_i \frac{r-r_0}{\rho_0}\right) dA = \int_{A_{die}} \varepsilon E^2 \, dA \tag{1}$$

where Y_i is the Young's modulus of ith membrane, r_0 is the neutral axis, ρ_0 is the radius of the curvature, ε is the permittivity of the dielectric membrane, and E is the applied electric field. Subscripts all and die stand for "all layers" and "dielectric membrane." Similarly, the equation of the moment equilibrium about the z-axis can be written as

$$\int_{A_{all}} \left(-Y_i \frac{r-r_0}{\rho_0}\right) r \, dA = \int_{A_{die}} \left(\varepsilon E^2\right) r \, dA \tag{2}$$

The film thicknesses, positions, stiffness (as a function of temperature), and geometries are used as inputs. We solve for r_0 and ρ_0. The tip deflection angle (the deflection at the free end, see the rightmost schematic in Figure 3a) is $\theta_{tip} = L\rho_0^{-1}$, where L is the initial length of the device.

Figure 3b shows as a color scale the tip deflection angle at the actuated state (for an electric field of 20 V µm⁻¹, and the SMPs in the soft state) versus the thickness of both SMP layers, for the device shown in Figure 1c. When the device bends, the first SMP layer (the layer closest to the DEA) is on the outside (highest tensile stress) and the second SMP is at the inside of the bending. As the structure is non-symmetric, the two SMP layers have drastically

ADVANCED
SCIENCE NEWS

www.advancedsciencenews.com

ADVANCED
FUNCTIONAL
MATERIALS

www.afm-journal.de

different effects on tip deflection: the first SMP layer has a higher stiffening effect on the bending than the second SMP. Increasing the thickness of either SMP layer decreases the actuation deformation. As depicted in the plots of stress versus cross-section position in Figure 3e (for the case corresponding to the black square in Figure 3b), the first SMP layer has the highest tensile stress. The legend of the stress plots is given in panel a. The neutral axis (zero stress) for this device is located in the second SMP layer, meaning that most of the DEA force is used to deform the first thinner SMP layer and the other non-SMP membranes.

Cooling down the SMPs fixes the actuation deformation into place, with a slight relaxation when the DEA voltage is removed. The sheet finds a new mechanical equilibrium for which we can write similar equilibrium equations of the force and the moment as we did for the actuation phase. In this equilibrium state, the compressive stress of the SMP layers is balanced by the tensile stress of the other membranes (Figure 3a). Figure S2, Supporting Information, compares the stress–strain–temperature behaviors of thermoresponsive SMPs and the materials without shape memory ability. Details regarding modeling along with some practical design considerations are included in the Supporting Information. Figure 3c plots the tip deflection angle in the latched state as a function of the two SMP thicknesses. Comparing Figure 3b,c, we see a reduction in tip deflection, and that the two SMP layers have markedly different effects on the actuation and latching performances. A thicker first SMP layer decreases the actuation deformation but enables latching with higher tip deflection. The second SMP layer alone is insufficient to lock the device; we need the first SMP layer to lock in a position. Figure 3f,g confirm the relaxation and the shape fixation phenomena. In the latched state, all non-SMP layers are still under tensile stress, held in place by the SMP layers. The stress in the first SMP layer goes from tensile (actuation state) to compressive (latched state) due to shape fixation. The relaxation of the device upon removing DEA voltage can be observed in the strain plots in Figure 3g; the strain in the actuation is higher than the strain in the latched state. The strain in first SMP layer has positive strain in the actuation state but negative in the latched state.

Finally, we compute an effective bending stiffness in the latched state as a proxy for the holding force. Both SMP layers play key role in determining this bending stiffness. We employed the usual form of Castigliano's first theorem[32] to the curved device with a tip deflection angle of 1.5π rad (inset of Figure 3d). The displacement of the curved beam (Δ_y) due to an external force of P can be expressed as

$$\Delta_y = \int_0^{\theta_{tip}} \left(\frac{M_{(\theta)}}{Y_i I_i} \frac{\partial M}{\partial P} \right) ds \qquad (3)$$

where M is the moment due to P, $Y_i I_i$ is the equivalent stiffness of the all layers with Y_i and I_i being the Young's modulus and the area moment of inertia of ith membrane, respectively. The bending stiffness of this curved beam is then found as $K_{bending} = P\Delta_y^{-1}$. Figure 3d shows the 2D plot of the bending stiffness versus thickness of the two SMP layers. The bending stiffness increases with the increase of both SMP thicknesses: high holding forces are in the top right of Figure 3d, but high deflections are obtained in a region near the bottom left.

To find a reasonable operating region, we first computed the SMP thicknesses for which the device can achieve a tip deflection angle > 300° (1.67π rad). The region fulfilling this requirement is enclosed by the yellow curve in Figure 3d. The SMP thicknesses for our devices are selected by the pair of values that give the highest bending stiffness within this region. The fabricated device shown in Figure 1b has 7 μm and 22 μm thick SMP layers, corresponding to the red square in Figure 3d. Both the experimental results and the model predictions show that the thickness of the SMP layers, the locations of the DEAs, the distance between the SMP layers, and the relative position of the shape locking materials (SMPs) to the other materials have major roles in the actuation and latching performances. Figure S4, Supporting Information, shows the model results for three different designs in which the layer order was varied, highlighting the importance of neutral axis location and careful choice of film stack sequence. This analytical model can be easily adapted for the multistable bending actuators to optimize their actuation, latching, or load-bearing capacities. The actuation part of this modeling can be used for all bending DEAs.

2.4. Experimental Validation of the Modeling Using the Tip Deflection Angle and Bending Stiffness

Our model requires knowing the Young's moduli of the membranes at room and at elevated temperatures. We carried out a dynamic mechanical analyzer (DMA Q800 from T.A. Instruments) on each material. Young's moduli versus temperature data is provided in Figure S3, Supporting Information. Sweeping temperature from 29 to 70 °C reduces the stiffness of the SMP by more than 200 times while the stiffness of the other materials decreases by approximately three times.

Figure 3. Modeling of the multistable dielectric elastomer sheets for the actuation, latching, and load-bearing states, and experimental validation. a) The leftmost three cross sections show the deflection for three different states. The close-ups show the stress distribution. In the "actuation" state, the DEA is on and the SMP is soft. In the "latched" state, the DEA is off and the SMP is rigid. The SMPs have compressive stress whereas the other layers are under a tensile stress. The rightmost schematic shows the tip deflection angle, the criterion used to quantify the deformation. b,c) The tip deflection angle plotted as a color scale as a function of the two SMP thicknesses, for the actuated and latched states. The SMP layers have different effects on the actuation and latching performances. d) Color plot of bending stiffness of a curved dielectric elastomer sheet (latched at 1.5π rad) versus the two SMP thicknesses. The inset shows the configuration used to determine the bending stiffness. The yellow line delimits the regions of SMP thicknesses where both the actuated and latched states have a deflection greater than 300° (1.67π rad). The SMP thicknesses of the device shown in Figure 1a is highlighted in red square. e,f) The stress profiles in each membrane at the actuation and latched states, for the device shown in Figure 1a at an actuation voltage of 5 kV. g) Strain versus position during actuation and after the device is latched. Strain in the actuation state decreases linearly from 10% to around 0%; the first SMP layer has the highest and second SMP layer have smallest deformation. When the device is latched, the strain relaxes in the non-SMP materials and first SMP layer then has compressive strain as opposed to tensile during actuation. h) Comparison of the experimentally measured tip deflections and model predictions, showing good agreement. i) Measured bending stiffness of a curved device, showing 4× higher stiffness in the latched state than at the soft actuated state.

We used the tip deflection angle as the validation parameter for our model. Figure 3h compares the model predictions with the experimental results for the case when the dielectric elastomer sheet was actuated at an elevated temperature (70 °C) and latched at 29 °C. 178° ($\approx\pi$ rad) tip deflection was measured at 5.5 kV at 70 °C where the model predicted a deflection of 197° ($\approx 1.11\pi$ rad). When the device was latched at the room temperature, it held most of its actuation deformation: following 5.5 kV actuation, 86% shape fixation was measured while the model predicted 83%.

Larger deformations can be obtained by further increasing the temperature, as the SMP becomes even softer. A tip deflection of 300° (1.67π rad) was obtained at 5 kV when the device was heated to 90 °C during actuation. Higher temperatures however increase heating and cooling times and increase the cross-heating between heater regions.

We measured the bending stiffness of the deformed dielectric elastomer sheet and compared with the analytical model. For the force measurement, the dielectric elastomer sheet was first actuated and locked at an angle of 180° (π rad). Two force measurements were carried out on this bent structure: one at the soft actuation state (the DEA and the SMP heating were on) and the other one at the latched state (both DEA and SMP heating were off). Figure 3i shows the measured bending stiffness of a deformed dielectric elastomer sheet at the actuation and the latched states. The bending stiffness of a device at a latched zero power state was ≈4.3 times higher than in the soft (hot) actuated state.

2.5. Gripping Objects with Different Shapes and Shape Fixation

To illustrate the versatility enabled by the shape reconfigurability, we first used the gripper to pick and place objects with two very different shapes (a circular screw and a horizontal tube), as shown in **Figure 4**a and Video S1, Supporting Information. The device was first actuated in a vertical bending shape to grip a circular plastic screw by softening the horizontal fibers. When the horizontal SMP fibers were softened, the stiff vertical SMP fibers (the effective stiff fibers) set the deformation mode. In Figure 4a, the soft fibers are shown in red and stiff fibers are in blue. After releasing the screw, the gripper was configured to pick a plastic tube by heating the vertical fibers, leaving the horizontal ones stiff. The gripper can thus alternate between different deformed shapes to easily grasp a range of objects.

Figure 4b and Video S2, Supporting Information, show the sequential deform-and-latch of three identical devices to illustrate shape fixation locked into different configurations.

Each device was first connected to the power supply, actuated, latched, and finally disconnected from the power supply. Each device had different latched configuration. The bottom row of Figure 4b shows the different stable deformed configurations of these three devices. The latched shapes could be used for example as reconfigurable RF antennas or optical reflectors, allowing devices to take on new beam shapes, without requiring any power to hold the new shapes.

When the SMPs are soft, the device can actuate quickly (can grasp object in seconds, limited here by the viscoelasticity of
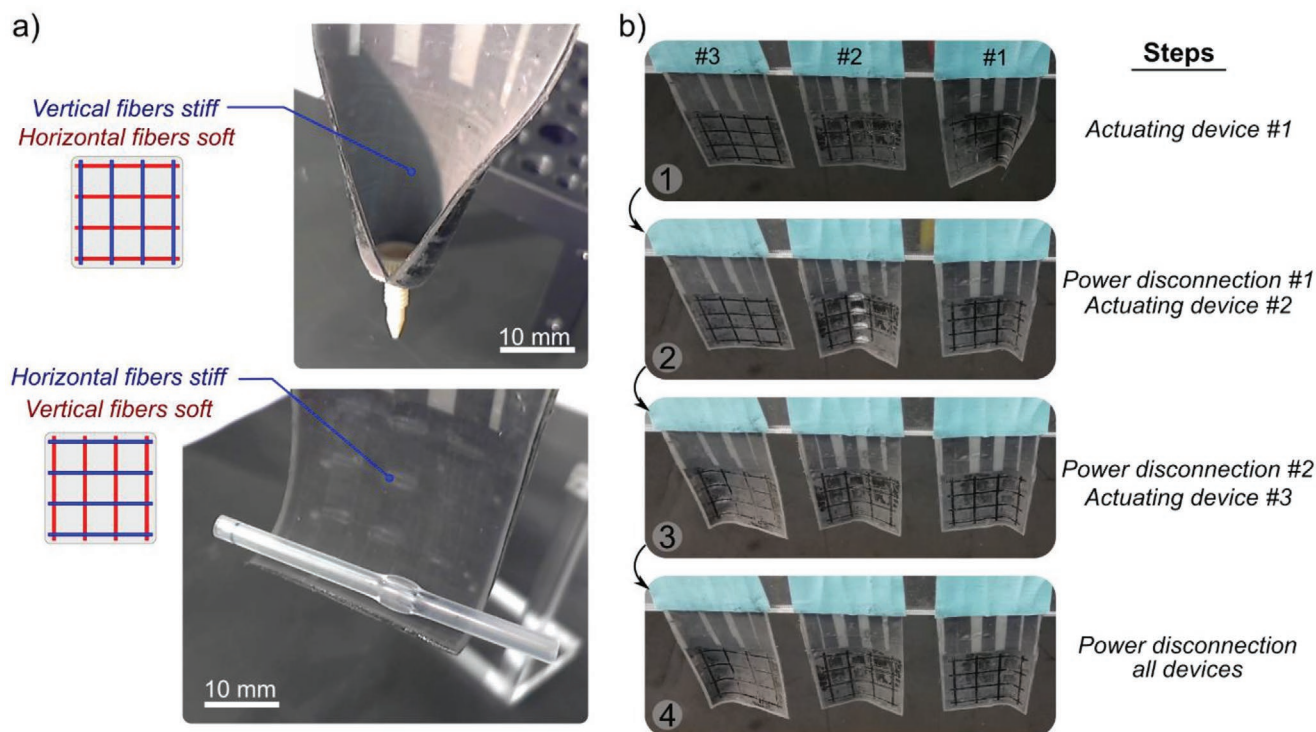

Figure 4. a) Gripping objects with very different shapes by heating either horizontal or vertical fibers to enable DEA actuation in vertical or horizontal axes. The horizontal SMP fibers are softened during actuation to wrap around a circular screw. The vertical fibers are then softened to pick-and-place a plastic tube (Video S1, Supporting Information). b) Shape fixation of three initially identical devices, showing examples of three stable sates after the electrical connection were removed (Video S2, Supporting Information). All three devices can recover their initial flat state by heating with no DEA voltage.

**ADVANCED
SCIENCE NEWS**
www.advancedsciencenews.com

**ADVANCED
FUNCTIONAL
MATERIALS**
www.afm-journal.de

the acrylic elastomer, could be much faster if using silicone elastomers).[17b,21a] Latching relies on passive cooling. For our dimensions, it takes tens of seconds to cool down below T_G. Latching is an essential property for long-term use at zero power, such as holding an object in place for long duration, or for smart delivery systems that hold a fixed shape fixed during transportation and recover their shape once at destination. Latching also enables more energy efficient system and it avoids the device breakdown due to applying high voltages for long periods.

2.6. Discussion on Designing Multistable DEA Using SMPs

This section presents qualitative outcomes of our model, to serve as a guide for designing multistable DEA sheets based on our architecture. We discuss on the thermomechanical properties of shape memory polymers that can improve the device performance.

Based on the modeling and experimental results, we suggest the following mechanical design rules for obtaining simultaneously large deformation and high holding force. The highest bending stiffness (blocked force) is achievable when two SMP layer are used (instead of one SMP layer) and they should locate at the outsides of the stacked layers so that the distance between them is greatest. This gives the highest area moment of inertia (as the cold SMP is the stiffest material).

Thicker SMP layers lead to higher blocked force. However, due to the limited force from the DEA, the thickness of the SMP layers and the location of the DEA should be chosen carefully. We found that the DEA can generate a high bending moment when the SMP layers have different thicknesses and when the DEA is placed close to the thinner one. The reason being that in this configuration, the neutral axis is close to the thicker SMP layer and the DEA is as far as possible from the neutral axis. Therefore, the bending moments (simply the DEA force times the distance between the DEA and the neutral axis) is maximum. This configuration results in the maximum strain in the thin SMP film and the minimum strain in the thick SMP layer (Figure 3g). As deforming thinner layers is easier, this gives a higher deflection.

If higher bending angles are required, a thin additional passive layer can be bonded to the outer side of the thick SMP layer to shift the neutral further away from the DEA, increasing the bending moment. The thickness of this layer is crucial as thick layer significantly increases the area moment of inertia during the actuation, so a careful balance must be found.

In addition to, or instead of, changing mechanical designs such as the layers order and thickness, the thermomechanical properties of the shape memory polymers can be tuned to increase the device performance. Among many options, thermoresponsive SMPs are good candidate for this application not only due to their high shape fixation ratio and shape recovery but also due to the very large stiffness change around their T_G. Based on their shape-fixing and shape-recovery mechanisms, Liu et al. classified SMPs into four main groups: 1) chemically cross-linked glassy thermosets, 2) chemically cross-linked semicrystalline rubbers, 3) physically cross-linked thermoplastics, and 4) physically cross-linked block copolymers.[33] Because

the performance of our DEA+SMP devices relies on a very high ratio of modulus below and above T_G (or T_M for crystalline cases), glassy thermosets and thermoplastics are the best options,[33,34] even though sharper transitions can be obtained from semicrystalline SMPs.

Lowering the SMP stiffness above T_G by changing the cross-linking density or by material synthesis would lead to higher actuation deformation. However, these changes must not decrease the stiffness at temperatures below T_G because this would decrease the holding force. Simply stated, using SMPs that are very stiff at $T < T_G$ and very soft at $T > T_G$) will maximize device performance. Shape memory polymers with sharp glass transition region will increase the speed of the device because only a small temperature change (ΔT) would be sufficient to switch states, reducing heating and cooling times.

3. Conclusion and Outlook

We combined a single soft actuator (a DEA) with a grid of shape memory polymers and an array of stretchable heaters to realise multistable and reconfigurable shape-morphing sheets. By addressing the integrated heaters, we can program local and temporary soft axes in different directions that allow dynamic control of multiple distinct deformations when the dielectric elastomer sheet is globally electrostatically actuated. We demonstrated more complex shape transformations by sequentially deforming and latching different regions. The shape memory polymers enabled holding the devices in the actuated shape with good blocking force once all voltages are removed.

The devices we report here could be fabricated using additive manufacturing techniques to reach higher resolution or further improve performance, for example by local thickness control of SMP or DEA. The device could be made faster by using photo-sensitive SMPs, or by embedding a microfluidic cooling systems. Dynamic control of shape change with latching ability can introduce multifunctionality and novel capabilities in soft devices.[14,35] Shape morphing sheet can be applied to soft robots to create, for example, reconfigurable wings and legs to adapt to different terrain or missions.

4. Experimental Section

The multistable dielectric elastomer sheets were made of stacked layers of acrylic elastomer, acrylic conductive elastomer, and shape memory polymer. The dielectric membranes were 250 µm thick acrylic elastomer (VHB 9473PC from 3M) and they were cut into 30 mm × 50 mm sheets. For the DEA and Joule heating electrodes, conductive acrylic materials (AR-care 90366 from Adhesives Research) were used. The thickness of conductive acrylic was 32 µm. The DEA electrodes were cut into 28 mm × 28 mm and placed on the opposite sides of the dielectric membranes, forming the active DEA region in Figure 1b. The fabricated device a buffer (passive) region located between the DEA region and the clamps. As this region is soft, it reduces the clamping effect on the DEA performance. The heating electrodes had a length of 28 mm and a varying width of a 5 and 0.5 mm. The narrow regions of the heaters were overlapped with the SMP segments. The electrodes are patterned using a laser cutter (8011 Speedy 300, from Trotec). To electrically insulate the heating electrodes, 50 µm thick acrylic elastomers (F9460PC from 3M) were used and they were cut into 30 mm × 50 mm sheets. As for the

SMP material, thermoplastic shape memory polyurethane (MM4520 from SMP technologies) was used. SMP membranes were fabricated using a similar method as previously reported.[36] Mixed SMP pellets were first mixed with dimethyl sulfoxide (DMSO, from Sigma-Aldrich) at a weight ratio of 1:4, then dissolved at 80 °C for 12 h. This mixture was casted on the top of a Teflon sacrificial layer. The DMSO was then evaporated at 80 °C in an oven for 1 h. The cured SMP membranes was patterned into grids using the laser cutter. Once all membranes were ready, they were laminated them to assemble the devices. Thanks to tackiness of the acrylic elastomers, no surface treatment was required to bond the membranes. Once assembled, markers were put at the bottom edge of the device which were tracked to measure the radius of the curvature. Some devices were coated with thermal dust (131F, from Solarcolordust.com), which helped us to get rid of the tackiness and image the hot region without the need of a thermal camera. For the validation experiments, a thermal camera (FLIR A50 from FLIR Systems, Inc.) was used to measure the temperature of the device.

To measure the radius of curvature, the markers were first tracked on the deformed images and then a circle was fitted to them using a custom Matlab code. Figure S5a, Supporting Information, shows two processed images where the circles were fitted to the tracked markers for undeformed and deformed states.

Supporting Information

Supporting Information is available from the Wiley Online Library or from the author.

Conflict of Interest

The authors declare no conflict of interest.

[1] E. Hawkes, B. An, N. M. Benbernou, H. Tanaka, S. Kim, E. D. Demaine, D. Rus, R. J. Wood, *Proc. Natl. Acad. Sci. USA* **2010**, *107*, 12441.

[2] Y. Liu, J. K. Boyles, J. Genzer, M. D. Dickey, *Soft Matter* **2012**, *8*, 1764.

[3] G. Z. Lum, Z. Ye, X. G. Dong, H. Marvi, O. Erin, W. Q. Hu, M. Sitti, *Proc. Natl. Acad. Sci. U. S. A.* **2016**, *113*, E6007.

[4] L. Hines, K. Petersen, M. Sitti, *Adv. Mater.* **2016**, *28*, 3690.

[5] a) Y. Liu, J. Genzer, M. D. Dickey, *Prog. Polym. Sci.* **2016**, *52*, 79; b) M. J. Ford, C. P. Ambulo, T. A. Kent, E. J. Markvicka, C. F. Pan, J. Malen, T. H. Ware, C. Majidi, *Proc. Natl. Acad. Sci.* USA **2019**, *116*, 21438; c) Z. S. Davidson, H. Shahsavan, A. Aghakhani, Y. B. Guo, L. Hines, Y. Xia, S. Yang, M. Sitti, *Sci. Adv.* **2019**, *5*, eaay0855.

[6] J. A. Faber, A. F. Arrieta, A. R. Studart, *Science* **2018**, *359*, 1386.

[7] a) A. A. Stanley, A. M. Okamura, *IEEE Trans. Haptics* **2015**, *8*, 20; b) N. Besse, S. Rosset, J. J. Zarate, H. Shea, *Adv. Mater. Technol.* **2017**, *2*, 1700102; c) Y. Qiu, Z. Y. Lu, Q. B. Pei, *ACS Appl. Mater. Interfaces* **2018**, *10*, 24807.

[8] R. Fernandes, D. H. Gracias, *Adv. Drug Del. Rev.* **2012**, *64*, 1579.

[9] J. M. McCracken, B. R. Donovan, T. J. White, *Adv. Mater.* **2020**, 1906564, https://doi.org/10.1002/adma.201906564.

[10] a) M. Shahinpoor, K. J. Kim, *Smart Mater. Struct.* **2001**, *10*, 819; b) R. Tiwari, E. Garcia, *Smart Mater. Struct.* **2011**, *20*, 083001.

[11] X. X. Le, W. Lu, J. W. Zhang, T. Chen, *Adv. Sci.* **2019**, *6*, 1801584.

[12] T. Guin, M. J. Settle, B. A. Kowalski, A. D. Auguste, R. V. Beblo, G. W. Reich, T. J. White, *Nat. Commun.* **2018**, *9*, 2531.

[13] B. A. Kowalski, V. P. Tondiglia, T. Guin, T. J. White, *Soft Matter* **2017**, *13*, 4335.

[14] T. H. Ware, M. E. McConney, J. J. Wie, V. P. Tondiglia, T. J. White, *Science* **2015**, *347*, 982.

[15] a) R. Pelrine, R. Kornbluh, Q. B. Pei, J. Joseph, *Science* **2000**, *287*, 836; b) C. Keplinger, T. F. Li, R. Baumgartner, Z. G. Suo, S. Bauer, *Soft Matter* **2012**, *8*, 285; c) S. Rosset, H. R. Shea, *Appl. Phys. Rev.* **2016**, *3*, 031105.

[16] a) H. Godaba, J. S. Li, Y. Z. Wang, J. Zhu, *IEEE Trans. Robot. Autom.* **2016**, *1*, 624; b) Y. Chen, H. Zhao, J. Mao, P. Chirarattananon, E. F. Helbling, N. P. Hyun, D. R. Clarke, R. J. Wood, *Nature* **2019**, *575*, 324; c) J. W. Zhao, J. M. Zhang, D. McCoul, Z. G. Hao, S. Wang, X. B. Wang, B. Huang, L. N. Sun, *Soft Robot.* **2019**, *6*, 713; d) X. B. Ji, X. C. Liu, V. Cacucciolo, M. Imboden, Y. Civet, A. El Haitami, S. Cantin, Y. Perriard, H. Shea, *Sci. Robot.* **2019**, *4*, eaaz6451.

[17] a) S. Shian, R. M. Diebold, D. R. Clarke, *Opt. Express* **2013**, *21*, 8669; b) L. Maffli, S. Rosset, M. Ghilardi, F. Carpi, H. Shea, *Adv. Funct. Mater.* **2015**, *25*, 1656.

[18] a) F. Carpi, C. Menon, D. De Rossi, *IEEE-ASME Trans. Mechatronics* **2010**, *15*, 460; b) C. J. Cao, X. Gao, A. T. Conn, *Adv. Mater. Technol.* **2019**, *4*, 1900128; c) P. Linnebach, G. Hau, G. Rizzello, S. Seelecke, *Proc. SPIE* **2019**, 10966.

[19] a) A. Marette, A. Poulin, N. Besse, S. Rosset, D. Briand, H. Shea, *Adv. Mater.* **2017**, *29*, 1700880; b) S. Biswas, Y. Visell, *Adv. Mater. Technol.* **2019**, *4*, 1900042; c) H. C. Zhao, A. M. Hussain, A. Israr, D. M. Vogt, M. Duduta, D. R. Clarke, R. J. Wood, *Soft Robot.* **2020**, https://doi.org/10.1089/soro.2019.0113.

[20] a) S. Shian, K. Bertoldi, D. R. Clarke, *Adv. Mater.* **2015**, *27*, 6814; b) J. Shintake, S. Rosset, B. Schubert, D. Floreano, H. Shea, *Adv. Mater.* **2016**, *28*, 231; c) G. K. Lau, K. R. Heng, A. S. Ahmed, M. Shrestha, *Appl. Phys. Lett.* **2017**, *110*, 182906.

[21] a) A. Poulin, M. Imboden, F. Sorba, S. Grazioli, C. Martin-Olmos, S. Rosset, H. Shea, *Sci. Rep.* **2018**, *8*; b) M. Imboden, E. de Coulon, A. Poulin, C. Dellenbach, S. Rosset, H. Shea, S. Rohr, *Nat. Commun.* **2019**, *10*; c) J. Costa, M. Ghilardi, V. Mamone, V. Ferrari, J. J. C. Busfield, A. Ahluwalia, F. Carpi, *Front. Bioeng. Biotechnol.* **2020**, *8*, 22.

[22] a) A. Lendlein, S. Kelch, *Angew. Chem., Int. Ed.* **2002**, *41*, 2034; b) M. Behl, M. Y. Razzaq, A. Lendlein, *Adv. Mater.* **2010**, *22*, 3388; c) Q. J. Ze, X. Kuang, S. Wu, J. Wong, S. M. Montgomery, R. D. Zhang, J. M. Kovitz, F. Y. Yang, H. J. Qi, R. K. Zhao, *Adv. Mater.* **2019**, 1906657, https://doi.org/10.1002/adma.201906657.

[23] a) X. F. Niu, X. G. Yang, P. Brochu, H. Stoyanov, S. Yun, Z. B. Yu, Q. B. Pei, *Adv. Mater.* **2012**, *24*, 6513; b) J. A. C. Liu, J. H. Gillen, S. R. Mishra, B. A. Evans, J. B. Tracy, *Sci. Adv.* **2019**, *5*, eaaw2897.

[24] A. Khaldi, J. A. Elliott, S. K. Smoukov, *J. Mater. Chem. C* **2014**, *2*, 8029.

[25] a) M. Behl, K. Kratz, J. Zotzmann, U. Nochel, A. Lendlein, *Adv. Mater.* **2013**, *25*, 4466; b) B. Aksoy, N. Besse, R. J. Boom, B. J. Hoogenberg, M. Blom, H. Shea, *Lab Chip* **2019**, *19*, 608.

[26] E. Hajiesmaili, E. Khare, A. Chortos, J. Lewis, D. R. Clarke, *Extreme Mech. Lett.* **2019**, *30*, 100504.

[27] a) G. Kofod, M. Paajanen, S. Bauer, *Appl. Phys. A* **2006**, *85*, 141; b) G. Kofod, W. Wirges, M. Paajanen, S. Bauer, *Appl. Phys. Lett.* **2007**, *90*, 081916; c) B. O'Brien, E. Calius, S. Xie, I. Anderson, *Proc. SPIE* **2008**, *6927*.

[28] a) M. Duduta, R. J. Wood, D. R. Clarke, *Adv. Mater.* **2016**, *28*, 8058; b) E. Hajiesmaili, D. R. Clarke, *Nat. Commun.* **2019**, *10*.

[29] a) D. McCoul, S. Rosset, N. Besse, H. Shea, *Smart Mater. Struct.* **2017**, *26*, 025015; b) C. T. Nguyen, H. Phung, T. D. Nguyen, H. Jung, H. R. Choi, *Sens. Actuator A-Phys.* **2017**, *267*, 505.

[30] G. G. Stoney, *Proc. R. Soc. A* **1909**, *82*, 172.

[31] T. Q. Lu, J. H. Huang, C. Jordi, G. Kovacs, R. Huang, D. R. Clarke, Z. G. Suo, *Soft Matter* **2012**, *8*, 6167.

[32] E. J. Hearn, *Mechanics of Materials*, Elsevier, New York **1997**.

[33] C. Liu, H. Qin, P. T. Mather, *J. Mater. Chem.* **2007**, *17*, 1543.

[34] L. Y. Wang, Y. Yang, Y. H. Chen, C. Majidi, F. Iida, E. Askounis, Q. B. Pei, *Mater. Today* **2018**, *21*, 563.

[35] A. S. Gladman, E. A. Matsumoto, R. G. Nuzzo, L. Mahadevan, J. A. Lewis, *Nat. Mater.* **2016**, *15*, 413.

[36] S. Rosset, O. A. Araromi, S. Schlatter, H. R. Shea, *J. Vis. Exp.* **2016**.